Journal of Alloys and Compounds 896 (2022) 162953

Contents lists available at ScienceDirect

Journal of Alloys and Compounds

journal homepage: www.elsevier.com/locate/jalcom

Ternary relation among stacking fault energy, grain size and twin nucleation size in nanocrystalline and ultrafine grained CuAl alloys

Shaojia Shi[a], Liangjuan Dai[b], Yonghao Zhao[b,*]

[a] State Key Laboratory of Supramolecular Structure and Materials, College of Chemistry, Jinlin University, Changchun 130012, China
[b] Nano and Heterogeneous Materials Center, School of Materials Science and Engineering, Nanjing University of Science and Technology, Nanjing 210094, China

ARTICLE INFO

Article history:
Received 15 September 2021
Received in revised form 18 November 2021
Accepted 24 November 2021
Available online 26 November 2021

Keywords:
Stacking fault energy
Grain size
Twin nucleation size
Cu and Cu-Al alloys
High-pressure torsion

ABSTRACT

The stacking fault energy γ of an alloy has been reported to significantly affect the grain size d and twin nucleation size r_c during grain refinement. However, ternary relation among γ, d and r_c has not been investigated comprehensively. Here we prepared nanocrystalline (NC) and ultrafine-grained (UFG) 99.99 wt% Cu, Cu-0.86 wt% Al and Cu-2.2 wt% Al alloys with different γ by high-pressure torsion (HPT), and then characterized d and r_c. Transmission electron microscopy observations show that under the same experimental condition d decreases and corresponding grain refinement mechanism transforms from dislocation subdivision to twin segmentation with decreasing γ. The relation among γ, d and r_c from experiments are consistent well with theoretical prediction from Meyers model. r_c decreases with decreasing d, and the variation is exacerbated by the decrease of γ. r_c increases first and then decreases by forming a peak-shaped variation with decreasing γ when d is in UFG regime, suggesting there exists an optimum stacking fault energy γ_c for twin nucleation. The r_c peak becomes flat and moves to higher γ value when d is in NC regime due to the enhanced geometric effect of d on r_c which weakens the role of γ. Our findings reveal a comprehensive ternary relationship among γ, d and r_c, and provide guidance for designing NC and UFG materials with high-density twins and good strength-ductility combination.

1. Introduction

Twinning and slipping are two competing grain refinement mechanisms in nanocrystalline (NC, < 100 nm) and ultrafine-grained (UFG, 100 nm – 1 μm) materials prepared by severe plastic deformation (SPD) [1]. The choice of grain refinement mechanisms is predominately governed by extrinsic deformation conditions and intrinsic nature of materials. The former case includes deformation strain, strain rate and temperature, etc. For the latter case, stacking fault energy (SFE) is one of the most crucial parameters [2,3]. It has been well acknowledged that in face-centered cubic (FCC) metals and alloys, twinning tendency is higher in materials with lower SFEs and vice versa. Moreover, the grain refinement mechanisms significantly affect the eventual microstructures such as grain size and thickness of twin lamellae, which usually determine the mechanical properties of NC and UFG samples [2,3]. The small grain size in NC and UFG materials results in a significantly higher yield strength than their coarse-grained (CG) counterparts due to the Hall-Petch relationship, but unfortunately this is accompanied with the expense of ductility [4,5]. Fortunately, both deformation twinning and pre-existing twin boundaries (TBs) have been reported as an effective strategy to enhance the ductility by retaining the dislocations accumulation capability and work hardening ability [6–9]. Therefore, it is of great significance to reveal the effects of SFE on grain size and thickness of twin lamellae in NC and UFG materials processed by SPD techniques.

Previous investigations suggest that for a material with a high SFE, grain refinement mechanisms are operated via dislocation subdivision and there usually exists a stable/equilibrium final grain size which decreases with decreasing SFE for FCC metals and alloys processed by SPD, e.g. ~200 nm for Cu (78 mJm^{-2} [10]) [11,12], ~350 nm for Ni (137–278 mJm^{-2} [13–15]) [16] and ~1.3 μm for Al (135–220 mJm^{-2} [17]) processed by equal-channel angular pressing (ECAP). The corresponding microstructure performs as block structured dislocation cells and lamellar grains, as a result of a balance between dislocation generation and annihilation [2]. For the materials with low SFEs, the final grain sizes also decreases with the reduction in SFE due to the enhanced interaction of high density twins, stacking faults (SFs) and microscale shear bands [18], e.g. 107 nm for Cu-5 at% Al (28 mJm^{-2}) and 82 nm for Cu-8 at% Al (17

* Corresponding author.
E-mail address: yhzhao@njust.edu.cn (Y. Zhao).

https://doi.org/10.1016/j.jallcom.2021.162953
0925-8388/

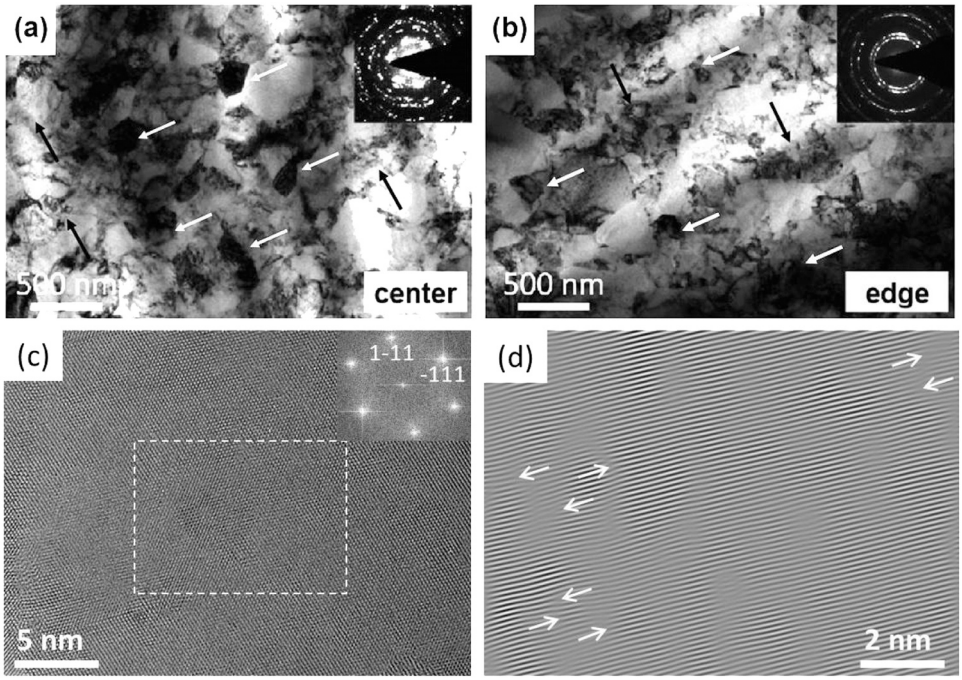

Fig. 1. (a,b) Bright-field TEM images taken from the center (a) and edge (b) of the HPT-processed Cu. Equiaxed nano-grains and ultrafine grains with clear grain boundaries are pointed out by white arrows, and dislocation cells are pointed out by black arrows. (c) [110] zone axis (Z.A.) HRTEM image of the HPT-processed Cu and the inset is the corresponding Fourier transformation (FFT) pattern. (d) The (1−11) inverse filtered Fourier transformation (IFFT) image of the region marked by white rectangle in (c), showing dislocation accumulation, as marked by white arrows.

mJm^{-2}) processed by four-pass ECAP [18]. Our previous transmission electron microscopy (TEM) observations in NC and UFG Cu and Cu-Zn alloys processed by high-pressure torsion (HPT) showed similar results [19,20]. For relation between twin thickness and SFE, Zhang et al. revealed that the twin thickness decreases with decreasing SFE, e.g. 25 nm for Cu-1 wt% Al with SFE of 61 mJm^{-2} and 12 nm for Cu-4.5 wt% Al with SFE of 12 mJm^{-2} processed by dynamic plastic deformation (DPD) at liquid nitrogen temperature (LNT). Such a relation originates from the reduced driving stress of twin nucleation and suppressed propagation of twins with the reduction of SFE [10]. Finally for relation between twin thickness and grain size, it has been reported that the twining behavior performs a strong correlation with the grain size due to the competition between deformation twinning and detwinning in NC regime. For example, Liao et al. revealed that the detwinning process prevails over the twinning process when the grain is smaller than a critical size, leading to thickness reductions of growth twins and deformation twins [3,21,22]. For nanocrystalline grains, twinning partials are emitted from grain boundaries (GBs) [3]. The critical grain size that allows these partial emissions is a function of SFE, i.e., decreasing SFE increases the critical grain size for partial emissions from GBs [23]. Therefore, from the above investigations, one can see only the simplified binary relationships between the three factors of SFE, grain size and twin thickness were focused and revealed. Considering any above binary relation between SFE, grain size and twin thickness might significantly affected by the third factor, thus the concrete ternary relation among SFE, grain size and twin thickness is very complicated and still lack in the literature.

In this work, to solve the above problem, 99.99 wt% Cu, Cu-0.86 wt% Al and Cu-2.2 wt% Al alloys with different SFEs were selected as model materials. HPT was employed to produce NC and UFG samples. The grain size distribution and thickness of twin lamellae were then characterized in hundreds of grains by extensive TEM and high-resolution transmission electron microscopy (HRTEM) analyses. Based on the TEM-measured results, the concrete ternary relation among SFE, grain size and twin nucleation size was finally appraised by Mohamed and Meyers models.

2. Materials and methods

The materials used in this work are pure Cu (purity 99.99 wt%) and Cu-Al alloys with Al concentrations of 0.86 and 2.2 wt%, respectively. According to Refs. [19,24,25], the SFEs of pure Cu and these Cu-Al alloys are approximately 78, 38 and 20 mJm^{-2}, respectively. Cu-Al alloy samples were prepared from high-purity components (99.99 wt% Cu and Al) by means of vacuum induction melting. Disks of Cu and Cu-Al alloys with a thickness of 1.2 mm and a diameter of 10 mm were processed via HPT for 5 revolutions at room temperature under an imposed pressure of 6.0 GPa and a rotational speed of 1 rpm. The samples were processed under quasi-constrained HPT where each disk was compressed between anvils resulting in a slight flow of material out the disk periphery during the torsion.

Specimens for TEM and HRTEM investigations were taken from the central area and at the edge of HPT-processed samples, and prepared using mechanical grinding followed by ion milling at LNT. TEM observations were conducted in an FEI-Tecnai G^2 20 S-TWIN microscope operated at 200 kV. HRTEM was conducted in a Titan G^2 60–300 operated at 300 kV.

3. Results

3.1. Microstructures of the HPT-processed Cu

Fig. 1a and b illustrate bright-filed TEM images taken from the center and edge of HPT-processed Cu sample. Both center and edge regions exhibit similar microstructures of equiaxed nano-grains and ultrafine grains with clear grain boundaries (GBs, pointed out by white arrows) homogeneously mixed with dislocation cells (pointed out by black arrows). The corresponding selected area electron

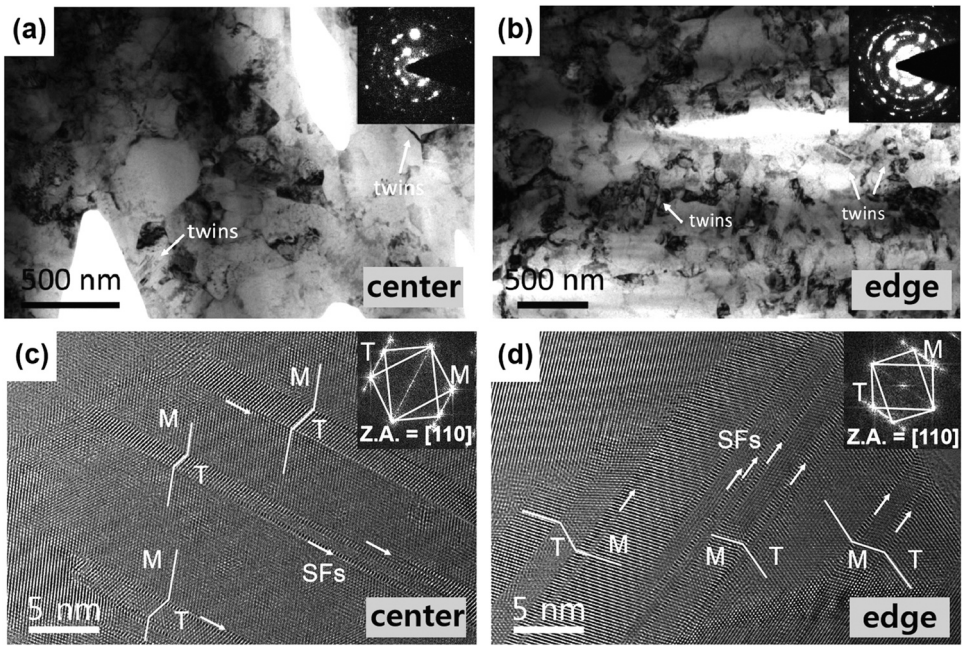

Fig. 2. (a,b) Bright-field TEM images taken from the central area (a) and edge (b) of HPT-processed Cu-0.86 wt% Al alloy. The twin lamellae were marked by white arrows and "T". (c,d) [110] zone axis (Z.A.) HRTEM images showing the twin lamellae (marked as "T") interspersed in the matrix ("M") and SFs (pointed out by white arrows) at the central area (c) and the edge (d) of the HPT-processed Cu-0.86 wt% Al sample, respectively. The corresponding FFT insets revealed the twin relationship.

diffraction (SAED) patterns show relatively continuous rings indicating that no obvious preferential grain orientations in the HPT-processed Cu samples.

Dislocation cells, observed in both regions, have the majority of dislocations tangling in the cell walls and fairly low-density of dislocations in cell interiors as a result of extensive dynamic recovery during the HPT process [2,26]. However, the cell size does not show an obvious reduction with increasing deformation strain, i.e. from central area to edge region. The cell size becomes stable by the balance between the dislocation multiplication and recovery processes above the critical strain [24]. As shown in the Fig. 1c and d, high density residual dislocations (marked by white arrows) tangle within the NC and UFG grains, suggesting the dislocation slipping dominates the deformation mechanism. It is worth noting that no deformation twins or stacking faults (SFs) were found in the HPT-processed Cu sample due to the high SFE (78 mJm^{-2}). The above results suggest that dislocation subdivision is the major grain refinement mechanism in Cu.

3.2. Microstructures of the HPT-processed Cu-0.86 wt% Al alloys

Fig. 2a and b show the typical TEM images of HPT-processed Cu-0.86 wt% Al alloy at center and edge, respectively. Compared with pure Cu sample, the grain sizes decrease (detailed statistics of grain size distributions are shown in Fig. 5) and the fraction of cell-like microstructures reduces. Besides, high-density nano-scale deformation twin lamellae (marked by white arrows and "T") were observed and further confirmed by corresponding HRTEM images. As shown in Fig. 2c and d, twin lamellae (marked by "T") with nano-scale thicknesses interspersed in the matrix and segmented the grain. Accompanying with twinning, massive SFs (marked by withe arrows) slipped along the TBs and within twin lamellae, acting as the potential twin nuclei for subsequent subdivision of the existed twin lamellae [3,27].

Comparing with central area shown in Fig. 2c, the twin density (detailed values are listed in Table 1) is higher and the segmentation by twin lamellae becomes more obvious at the edge as shown in Fig. 2d, due to the higher strain at the edge in the HPT-processed Cu-0.86 wt% Al sample. The low SFE of Cu-0.86 wt% Al alloy (38 mJm^{-2}) promotes the dissociation of unit dislocation into partials, thereby inducing high density of twin lamellae and massive SFs during the HPT process.

3.3. Microstructures of the HPT-processed Cu-2.2 wt% Al alloys

As shown in Fig. 3a and b, the microstructures of HPT-processed Cu-2.2 wt% Al alloy perform similar feature with those of the HPT-processed Cu-0.86 wt% Al alloy, containing homogeneously distributed equiaxed nano-grains and ultrafine grains as well as nano-scale twin lamellae (marked by white arrows and "T"). Large number of TEM observations show that the grain sizes are smaller and the twin density becomes higher in Cu-2.2 wt% Al than those in Cu-0.86 wt% Al with lowering SFE from 38 mJm^{-2} (Cu-0.86 wt% Al) to 20 mJm^{-2} (Cu-2.2 wt% Al). The detailed measured twin densities are listed in Table 1. As shown in Fig. 3c and d, the typical [110] Z.A. HRTEM images taken from the central area and the edge region of HPT-processed Cu-2.2 wt% Al alloy respectively, consecutive nano-scale twin lamellae with rough TBs divides the grain matrix, accompanying with massive SFs at TBs. The results indicate a severe segmentation by twin lamellae, and twinning performs an important grain refinement mechanism in the HPT-processed Cu-2.2 wt% Al alloy.

Accompanied with deformation twins, SF is another important deformation mechanism in the Cu-0.86 wt% Al and Cu-2.2 wt% Al alloy. As shown in Fig. 4, consecutive SFs pointed out by with arrows emitted from a GB marked by white dotted line and passed through nano-scale twin lamellae in HPT-processed Cu-0.86 wt% Al (Fig. 4a and b) and Cu-2.2 wt% Al (Fig. 4c and d) alloys, indicating deformation twinning is operated via partial dislocation emission from GBs. These results are consistent with our former investigations in the NC and UFG Cu-30% Zn alloy [28]. According to the literature, dislocation-based mechanisms in grain interior [29] were proposed to explain twin nucleation in coarse-grained FCC materials. Once the grain sizes decrease to the NC and UFG regimes, the applied flow stress is hard to satisfy the activation for the grain interior Frank-Read or Köhler [30,31] source and the conventional dislocation-

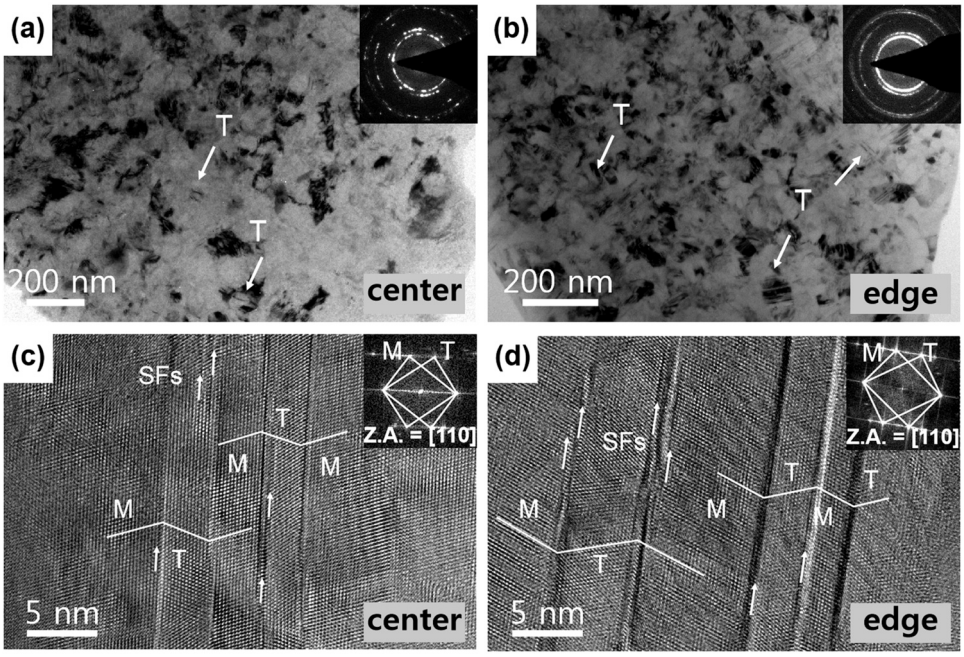

Fig. 3. (a,b) Bright-field TEM images taken from the central area (a) and edge region (b) of HPT-processed Cu-2.2 wt% Al alloy. The twin lamellae were marked by white arrows and "T". (c,d) [110] zone axis (Z.A.) HRTEM images showing the twin lamellae (marked as "T") interspersed in the matrix ("M") and SFs (pointed out by white arrows) at the central area (c) and the edge region (d) of the HPT-processed Cu-2.2 wt% Al sample, respectively. The corresponding FFT insets revealed the twin relationship.

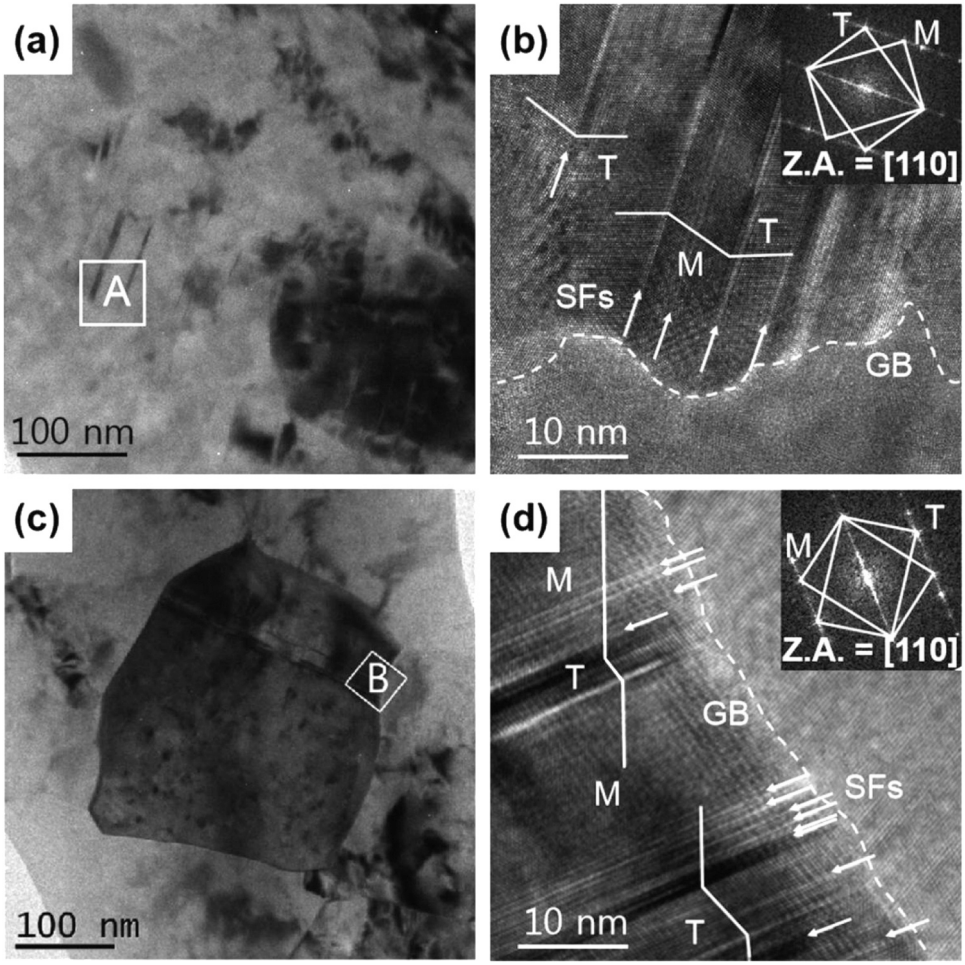

Fig. 4. (a,c) Bright-field TEM images at the edge of HPT-processed Cu-0.86 wt% Al and Cu-2.2 wt% Al alloys, respectively. (b,d) [110] zone axis (Z.A.) HRTEM images of the regions A in (a) and B in (c) (marked by white rectangle and diamond, respectively), showing twinning via consecutive SFs emission from GBs. The corresponding FFT patterns of insets revealed the twin relationship.

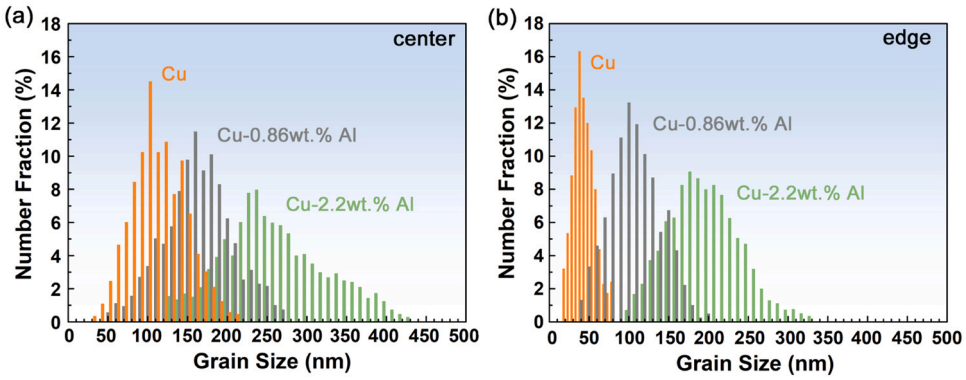

Fig. 5. Statistical grain size distributions at central area (a) and edge (b) of HPT-processed Cu, Cu-0.86 wt% Al and Cu-2.2 wt% Al alloys, respectively. The linear intercept was used to measure the grain sizes and about 300 grains were measured for each sample.

Table 1
A list of the TEM-measured average grain size d, twin density ρ at the center and edge of HPT-processed Cu, Cu-0.86 wt% Al and Cu-2.2 wt% Al alloys.

Samples	Cu		Cu-0.86 wt% Al		Cu-2.2 wt% Al	
Region	center	edge	center	edge	center	edge
d (nm)	230	170	150	100	105	45
ρ (%)	0	0	12.3	15.1	15.7	17.9

based twinning mechanisms cease to operate [32]; instead, the GB-mediated twinning mechanism by the consecutive SFs emission from GB starts to dominate [33].

Fig. 5 shows the statistical grain size distributions at center (Fig. 5a) and edge (Fig. 5b) of the HPT-processed Cu, Cu-0.86 wt% Al and Cu-2.2% wt% Al, determined from a large number of TEM images. The corresponding average grain sizes d and twin density ρ are listed in Table 1. It can be seen that, with decreasing SFE, d and the width of the grain size distribution at the same region are decreased to some extent. This indicates that the grain structure becomes more uniform with decreasing SFE. In addition, ρ increases with the SFE reduction and deformation strain (i.e. from center to edge), suggesting twinning plays an important role in the grain refinement of Cu-0.86 wt% Al and Cu-2.2 wt% Al alloys during HPT process.

4. Discussion

4.1. Effect of SFE on grain size

Previous studies have revealed that the final stable/equilibrium average grain size d obtained by the SPD-induced grain refinement is governed by many factors, mainly including the external factors, e.g. loading modes, strain magnitude, temperature and strain rate, and intrinsic factors, e.g. hardness, SFE, melting point, activation energy and bulk modulus [2,18,24]. In our early investigations, it was revealed that d decreases by lowering the SFE in HPT-processed Cu and Cu-Zn alloys [19]. As listed in Table 2, the decrease in the SFE leads to a decrease in d in the order of Cu to Cu-0.86 wt% Al and Cu-2.2 wt% Al after processing by HPT under the same experimental condition. This tendency is consistent with data observed in mechanical-milling processed metals and alloys, and it is explained by the concept that d is determined by a dynamic balance between dislocation generation and recovery in Mohamed model [34]. Thus, lowering SFE promotes the planar slip and the dissociation of unit dislocations, and consequently suppresses cross-slip and recovery process [35–37], leading to smaller d. What's more, the lower SFE results in higher twinning density listed in Table 1, and the segmentation of twin lamellae (shown in Figs. 2c, d, 3c and d) provides an additional effective refinement mechanism except dislocation subdivision, contributing to grain refinement [18,38].

Table 2
A list of the TEM-measured average grain sizes d, lattice parameters a, SFE γ, Burgers vectors of unit dislocation b, partial dislocation b_p and shear modulus G of HPT-processed Cu, Cu-Al alloys (Cu-0.86 wt% Al and Cu-2.2 wt% Al) and Cu-Zn alloys (Cu-10 wt % Zn and Cu-30 wt% Zn).

Samples	Cu [19]	Cu-0.86 wt% Al [22]	Cu-2.2 wt% Al [23]	Cu-10 wt% Zn [19]	Cu-30 wt% Zn [19]
d (nm)	200	120	60	/	/
a (Å)	3.619	3.621	3.623	3.641	3.691
γ (mJm^{-2})	78	38	20	35	14
b (nm)	0.2559	0.2561	0.2562	0.2575	0.2610
b_p (nm)	0.1477	0.1478	0.1479	0.1487	0.1507
G (GPa)	48.30	47.85	47.18	46.5	40.1

Based on Mohamed model, the relationship between d and SFE γ is expressed as [34]:

$$\frac{d}{b} = A\left(\frac{\gamma}{Gb}\right)^{0.5} \quad (1)$$

Where b is the Burgers vector of unit dislocation, A is a constant and G is the shear modulus. For a FCC structure, b is the length of unit dislocation along the < 110 > direction and equal to $\sqrt{2}a/2$, where a is the lattice parameter. The values of a, b, γ and G for Cu to Cu-0.86 wt% Al and Cu-2.2 wt% Al are listed in Table 2. Fig. 6 shows a plot of d/b versus γ/Gb on a logarithmic scale by TEM-measured data. Inspection shows that the two terms do not scale with each other in a linear way. Moreover, if it is assumed that this non-linearity is

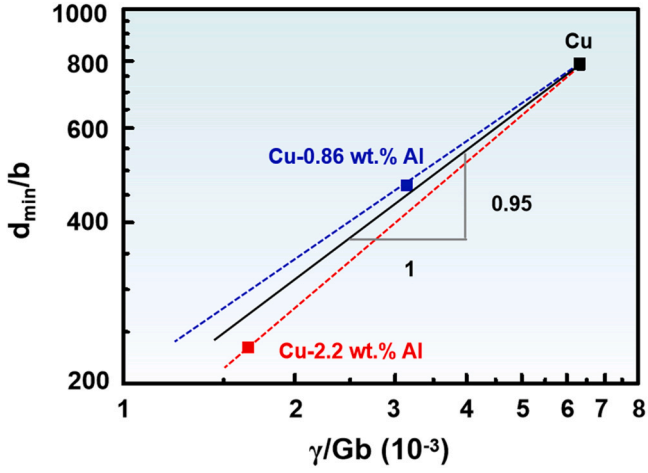

Fig. 6. Plot of d/b vs γ/Gb on the logarithmic scale showing that the two terms do not scale linearly and the slopes of 0.95 from the TEM results deviate from the value of 0.5 predicted in Eq. (1).

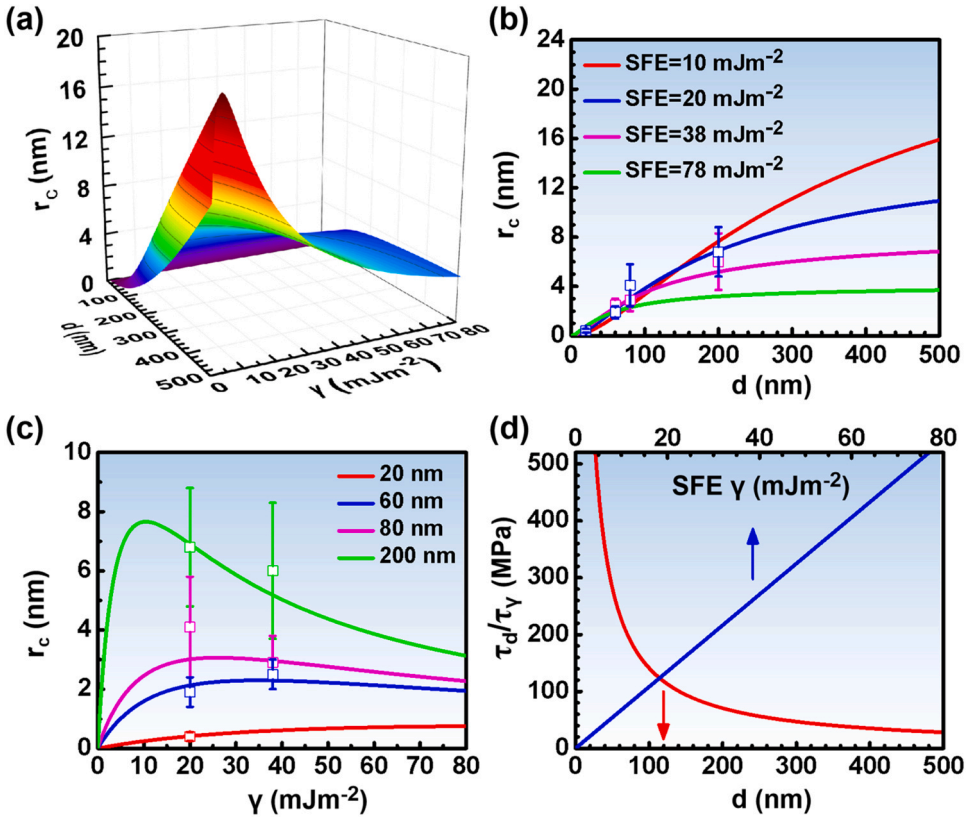

Fig. 7. (a) Three dimensional diagram showing the relationship among grain size d, SFE γ and twin nucleation size r_c for Cu-Al alloys. (b) Cross-sectional diagram showing the relationship between d and r_c for Cu-0.86 wt% Al (38 mJm^{-2}) and Cu-2.2 wt% Al (20 mJm^{-2}) alloys. (c) Cross-sectional diagram showing the relationship between γ and r_c with d = 200, 80, 60 and 200 nm. The data points in (b) and (c) are TEM-measured average twin thickness. (d) Relationships among the twinning shear stress τ (τ_d/τ_γ), d and γ.

caused by scattering in the data, it is possible to fit the data with straight lines (marked by black line) as shown in Fig. 6 to yield slope of 0.95 from the TEM measured d. The slope is significantly higher than the slope of 0.5 predicated in the model in Eq. (1). This disagreement is reasonable when it is noted that the model is based on the occurrence of a single deformation mechanism of dislocation slip, whereas, as shown in Figs. 1–3, Cu deformed primarily by single dislocation slip in this investigation while Cu-0.86 wt% Al and Cu-2.2 wt% Al deformed by multiple deformation mechanisms including dislocation slip, twinning and SFs. The multiple deformation mechanisms were more effective for the grain refinement, leading to a greater slope. What's more, the slope (marked by red dotted line) between Cu and Cu-2.2 wt% Al alloy is higher than the slope (marked by blue dotted line) between Cu and Cu-0.86 wt% Al, indicating the higher density twin contributes more plastic deformation in the grain refinement process.

From the perspective of energy, d is closely related to the activation energy for diffusion Q [34,39]. The relationship between d and Q is given by [18,38]:

$$\frac{d}{b} = 112e^{-0.0037Q} \tag{2}$$

This suggests that d decreases by increasing Q during deformation. Q can be affected remarkably by the degree of coincidence of GBs [40]. General GBs constitute a region of lattice distortion, resulting in diffusion along a boundary that becomes more favorable as this distortion increase [40]. However, the diffusion may be delayed for certain boundaries whose atom arrangement is highly regular, such as TBs, leading to the enhancement of Q [18]. Owing to low SFE, these highly regular TBs form readily at the initial stage of deformation, enhancing the tendency to increase Q. In other words, lowering the SFE to some extent is equivalent to increasing Q, consequently decreasing d under the same experimental condition.

It should be noted that though twinning plays an important role in grain refinement, the smallest average grain size doesn't necessarily equal the smallest TB spacing. For example, Cao et al. [41] found the smallest average grain size achieved in a duplex stainless steel by HPT is ~23 nm, which is much larger than the average primary TB spacing of 7 nm [42]. Detailed investigation revealed that de-twinning of the primary twins occurred and produced high densities of sessile dislocations, of which accumulation further produces new low angle GBs [41]. These results suggest that for materials with very small SFEs, not only twinning but also detwinning occurred during SPD process, which makes the effect of SFE on grain refinement more complicated.

4.2. Influences of grain size and SFE on twin nucleation size

It has been widely acknowledged that the twin nucleation induced by plastic deformation is affected by two intrinsic factors: grain size d and SFE γ [31]. Meyers et al. proposed the GB-mediated twinning model to predict the critical twin nucleus size, in which it was assumed that the twin embryo is a ellipsoidal (oblate spheroid) nucleus with radius r_c and thickness λ_c, and a constant aspect ration ρ ($\rho = \lambda_c/r_c$) [31]. The twin embryo size r_c is directly related to γ and twinning driving stress (i.e. the critical resolved shear stress for deformation twinning)σ_T, as expressed by [31]:

$$r_c = \frac{5\pi G\gamma_{CTB}}{4\sigma_T^2} \tag{3}$$

where G is the shear modulus, $\gamma_{CTB} = 0.75\gamma$ is coherent TB energy. Furthermore, in UFG materials σ_T could be calculated by the shear

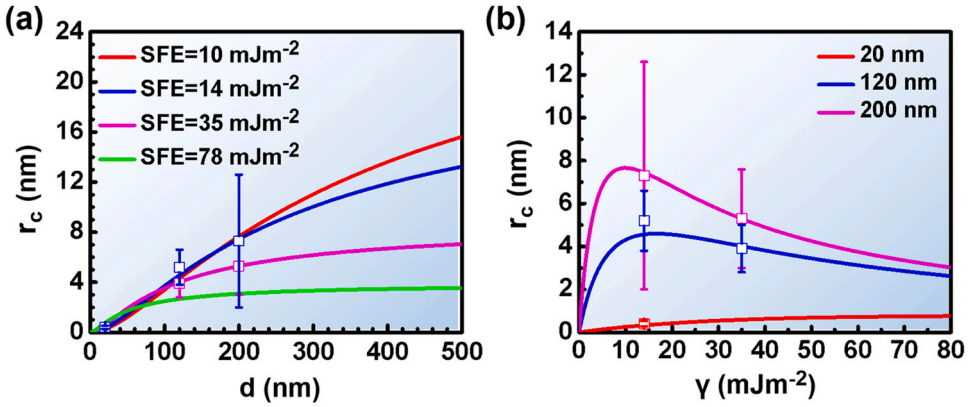

Fig. 8. (a) The cross-sectional diagram showing the relationship between d and r_c for Cu-10 wt% Zn (35 mJm^{-2}) and Cu-30 wt% Zn (14 mJm^{-2}) alloys. (b) The cross-sectional diagram showing the relationship between γ and r_c. d are chosen as 200, 120 and 20 nm. The data points in (a) and (b) of the corresponding TEM-measured average twin thickness were obtained from Refs. [28,45,46].

stress τ_T, which directly drives partial dislocations, i.e. SFs, for twinning nucleation [43,44]. The relationship is expressed as:

$$\sigma_T = 3.1\tau_T \tag{4}$$

$$\tau_T = \frac{2\alpha G b_p}{d} + \frac{\gamma}{b_p} \tag{5}$$

where the parameter α is a constant ($\alpha = 0.5$ and 1.5 for edge and screw dislocations respectively) [29], $b_P$is Burgers vector of Shockley partial dislocation as listed in Table 2. According to the Eq. (5), it is clearly that $\tau_T$depends on two parts of d effect $\tau_d(\tau_d = \frac{2\alpha G b_p}{d})$ and γ effect $\tau_\gamma(\tau_\gamma = \frac{\gamma}{b_p})$. By substituting Eqs. (4) and (5) into Eq. (3), the following equation is obtained:

$$r_c = \frac{3.75\pi G\gamma}{38.44 \times \left(\frac{2\alpha G b_p}{d} + \frac{\gamma}{b_p}\right)^2} \tag{6}$$

For Cu-Al alloys in this study, the values of G and $b_P$could be approximated to constants, due to the extremely small variations (as listed in Table 2). Consequently, by substituting the values of G and b_P in Eq. (6), the three dimensional diagram can be obtained, as shown in Fig. 7a, revealing the theoretical relationship between d, γ and r_c for Cu-Al alloys.

4.2.1. Influences of grain size on twin nucleation size

For the specific Cu-0.86 wt% Al (38 mJm^{-2}) and Cu-2.2 wt% Al (20 mJm^{-2}) alloys, the binary relationship between d and r_c is shown in Fig. 7b. Based on the GB-mediated twinning model [31], once twin nucleus is formed, it grows in a manner of self-similar twin growth with r_c increasing in proportion to λ_c. Therefore, the thickness λ_c of twin nucleus also reflects the radius r_c. In Figs. 7 and 8, we simply and qualitatively describe the measured twin width as the radius r_c. It can be seen that r_c decreases and the decreasing velocity accelerates with decreasing d. The lower γ is, the more obvious the decreasing tendency is. Furthermore, the measured twin thickness with d = 200, 80, 60 and 20 nm is in good agreement with theoretically predicted values within the error bar. In addition, Meyers model described by Eq. (6) about twin nucleation was also applied in Cu-10 wt% Zn (35 mJm^{-2}) and Cu-30 wt% Zn (14 mJm^{-2}) alloys. The corresponding cross-sectional diagram of the relationship between d and r_c is shown in Fig. 8a. The experimental data points were obtained from Refs. [28,45,47] and are also consistent with the theoretically prediction. It is true that the deformed twin thickness depends on two processes of nucleation and growth, but r_c determines the thickness of twin lamellae to a large extent [10]. So, it is reasonable to evaluate the twin thickness by r_c.

From the perspective of force, r_c reflects the required driving shear stress for twin nucleation. According to the Eq. (5), τ_T could be divided into two cooperation parts of the grain size effect τ_d ($\tau_d = \frac{2\alpha G b_p}{d}$) and the SFE effect $\tau_\gamma(\tau_\gamma = \frac{\gamma}{b_p})$. The former τ_d increases with decreasing d, and the latter τ_γ increases with increasing γ [3,33,47]. For the Cu-Al alloy system shown in Fig. 7d, τ_d and the accelerated velocity increase with decreasing d, and $\tau_d$gradually dominates the driving shear stress for twin nucleation. The variation of τ_d with d indicates that the difficulty of twin nucleation increases with decreasing d, especially in the NC regime, because twin nucleation requires that the applied flow stress is higher than stresses for emitting both leading Shockley partial and twinning partial dislocations which also increase with decreasing d [3]. As d is below a certain critical grain size d_c, the required stress for twinning is larger than that for emitting leading partial dislocation [47] and twinning is then suppressed. In this case, only extended SFs can be activated. From another perspective, such tiny grain ($d < d_c$) only has space to contain single atomic-layered SFs and has insufficient room to contain the twin embryos [3,28]. For Cu-2.2 wt% Al when d = 20 nm, as shown in Fig. 7b, the theoretical predicted r_c is 0.37 equal to the thickness of SFs. Our TEM observation also verified that no twins and only SFs can be discerned when d < 20 nm in Cu-2.2 wt% Al (Fig. 7b) and Cu-30 wt% Zn (Fig. 8a) [28]. These results suggest that Meyers model can be generalized into NC regime because the single atomic-layered SF in tiny grains ($d < d_c$) could also be regarded as a specific twin embryo.

4.2.2. Influence of SFE on twin nucleation size

To further reveal the relationship between γ and r_c, the cross-sectional curves were also taken by selecting d = 200, 80, 60 and 20 nm. As shown in Fig. 7c, with decreasing SFE, r_c increases first and then decreases sharply by forming a peak-shaped variation when d is in UFG region. The r_c peak becomes flat and moves to higher γ value when d decreases from UFG to NC region. The theoretical curve suggests that there is an optimum SFE γ_c for twin nucleation for a specific grain size. When d = 200, 80, and 60 nm, γ_c are 10, 26, and 34 mJm^{-2} respectively, indicating that γ_c increases with decreasing d. The experimental data in Fig. 7c are the average twin lamellae thickness with d = 200, 80 and 60 nm, respectively, and are consistent with the theoretical values. Furthermore, for the Cu-10 wt% Zn (35 mJm^{-2}) and Cu-30 wt% Zn (14 mJm^{-2}) alloys, r_c performs the similar tendency with γ and the experimental data points (obtained from Refs. [28,45,46]) are consistent with the theoretical prediction,

as shown in Fig. 8b. This is first report that inverse relationship between r_c and γ.

When γ is high, for example, > 50 mJm^{-2}, the dissociated partial dislocations prefer to constrict to a unit dislocation and then cross slip, because the higher the SFE is, the smaller the width of the extended dislocation is. In this case, the applied flow stress is relieved by cross slip and hard to reach the twinning stress. With lowering γ but γ is still larger than γ_c, the energy barrier of the unit dislocation dissociation decreases, promoting the emission and slip of partial dislocations [36]. Therefore, r_c and the thickness of twin lamellae increase due to the successive emission of partial dislocations on the adjacent (111) planes. With further decreasing γ below γ_c, single SF is promoted and then delays twin formation, because single SF preferentially relieves the local stress concentration that is needed for subsequent twin nucleation [10]. Meanwhile, the extremely low SFE dramatically increases the probability of single atomic-layered SFs acting as the potential twinning nucleation site, which may lead to high density twin nuclei [10]. These nuclei will compete with each other for growth. So the individual twin nucleus size r_c decreases in the finite grain space when the SFE is lower than the optimum SFE γ_c.

It can be seen in Fig. 7c that d has an evident influence on the relationship between γ and r_c. UFG grains have enough space to accommodate the variation of r_c versus γ, which enhances γ effect on r_c, i.e. the corresponding curve varies more obviously for larger UFG grain. Meanwhile, the larger d delays the competition of high density twin nuclei, thereby decreasing γ_c. With decreasing d down to NC regime, the variation of r_c against γ becomes smooth. As shown in Fig. 7d, the twinning stress τ_d is far greater than τ_γ in the NC regime and dominates the twinning nucleation. Consequently, the γ effect on twin nucleation is weakened with decreasing d. In addition, γ_c increases with the decrease of d, suggesting that twinning can still nucleate in the NC materials with high SFEs. The previous molecular dynamics simulations and TEM observations have confirmed the nano-scale deformation twin lamellae in NC Al (135–220 mJm^{-2}), and Ni (137–278 mJm^{-2}) samples [48–50]. These results validate the feasibility and effectiveness of the relationship between γ and r_c in this work.

In addition to grain size and SFE, the thickness of twin lamella is also affected by deformation conditions. Zhang et.al reported that the thickness of twin lamellae in NC Cu-Al alloys by DPD at LNT, decreases with the decreasing SFE [10]. The d of NC Cu-Al alloys by DPD ranges from 25 to 50 nm [24], thereby the extremely small grain size might result in a high γ_c. Furthermore, γ is affected remarkably by the temperature, and decreases by 20–60% when the temperature decreases from room temperature to LNT [51,52]. Thus, γ_c is significantly higher than the actual SFE of LNT-DPD-processed Cu-Al alloys. So the thickness of twin lamellae decreased with the decrease of SFE in the LNT-DPD-processed Cu-Al alloys [10,24].

5. Conclusions

In this study, NC and UFG 99.99 wt% Cu, Cu-0.86 wt% Al and Cu-2.2 wt% Al alloys with different SFEs were prepared by HPT and the corresponding grain size distribution and thickness of twin lamellae were characterized by TEM. Based on the TEM-measured results, the interactive effects between d, γ and r_c were explored by Mohamed and Meyers models. The main conclusions are as follows:

1. The grain size decreases with decreasing SFE under the same experimental condition and the variation dose not follow the Mohamed model based on the single deformation mechanism of dislocation slip. The deviation results from the higher density twin with lower SFE, providing more plastic deformation in the grain refinement process.
2. TEM observation indicated that the twin nucleation size r_c decreases with decreasing grain size for Cu-0.86 wt% Al and Cu-2.2 wt% Al alloys, agreeing with Meyers model. The high twinning stress σ_T in tiny NC grain ($d < d_c$) hinders the twinning nucleation, and in this case, only single atomic-layer SFs can be activated.
3. The Meyers model applied in Cu-Al and Cu-Zn alloys reveals a peak shaped variation of twin nucleus size r_c against SFE with an optimum SFE γ_c for twin nucleation under a specific grain size. With the decrease of grain size from UFG to NC region, the geometric effect of grain size on twin nucleation size r_c is enhanced, weakens the influence of SFE and increases the optimum SFE γ_c.

Declaration of Competing Interest

The authors declare that they have no known competing financial interests or personal relationships that could have appeared to influence the work reported in this paper.

Acknowledgements

Y.H. Zhao acknowledges financial supports from National Key R& D Program of China (Grant No. 2017YFA0204403) and the National Natural Science Foundation of China (Grant No. 51971112 and 51225102) as well as the Fundamental Research Funds for the Central Universities, China (Grant No. 30919011405).

Conflict of Interest

The authors declare no conflict of interest.

References

[1] J.W. Christian, S. Mahajan, Deformation twinning, Prog. Mater. Sci. 39 (1995) 1–157.
[2] Y. Cao, S. Ni, X.Z. Liao, M.S., Y.T. Zhu, Structural evolution of metallic materials processed by severe plastic deformation, Mater. Sci. Eng. R 133 (2018) 1–59.
[3] Y.T. Zhu, X.Z. Liao, X.L. Wu, Deformation twinning in nanocrystalline materials, Prog. Mater. Sci. 57 (2012) 1–6.
[4] I.A. Ovid'ko, R.Z. Valiev, Y.T. Zhu, Review on superior strength and enhanced ductility of metallic nanomaterials, Prog. Mater. Sci. 94 (2018) 462–540.
[5] Y.H. Zhao, Y.T. Zhu, E.J. Lavernia, Strategies for improving tensile ductility of bulk nanostructured materials, Adv. Eng. Mater. 12 (2010) 769–778.
[6] L. Lu, Y.F. Shen, X.H. Chen, L.H. Qian, K. Lu, Ultrahigh strength and high electrical conductivity in copper, Science 304 (2004) 422–426.
[7] K. Lu, L. Lu, S. Suresh, Strengthening materials by engineering coherent internal boundaries at the nanoscal, Science 324 (2009) 349–352.
[8] L. Lu, X. Chen, X. Huang, K. Lu, Revealing the maximum strength in nanotwinned copper, Science 323 (2009) 607–610.
[9] Y.H. Zhao, Y.T. Zhu, X.Z. Liao, Z. Horita, T.G. Langdon, Tailoring stacking fault energy for high ductility and high strength in ultrafine grained Cu and its alloy, Appl. Phys. Lett. 89 (2006) 121906.
[10] Y. Zhang, N.R. Tao, K. Lu, Effect of stacking-fault energy on deformation twin thickness in Cu-Al alloys, Scr. Mater. 60 (2009) 211–213.
[11] F.D. Torre, R. Lapovok, J. Sandlin, P.F. Thomson, C.H.J. Davies, E.V. Pereloma, Microstructures and properties of copper processed by equal channel angular extrusion for 1–16 passes, Acta Mater. 52 (2004) 4819–4832.
[12] S. Komura, Z.J. Horita, M. Nemoto, T.G. Langdon, Influence of stacking fault energy on microstructural development in equal-channel angular pressing, J. Mater. Res. 14 (1999) 4044–4050.
[13] C. Brandl, P.M. Derlet, H.V. Swygenhoven, General-stacking-fault energies in highly strained metallic environments: ab initio calculations, Phys. Rev. B 76 (2007) 054124.
[14] I.L. Dillamore, R.E. Smallman, The stacking-fault energy of F.C.C metals, Philos. Mag. 299 (1964) 191–193.
[15] C.B. Carter, S.M. Holmes, The stacking-fault energy of nickel, Philos. Mag. 35 (1977) 1161–1172.
[16] A.P. Zhilyaev, B.K. Kim, J.A. Szpunar, M.D. Baró, T.G. Langdon, The microstructural characteristics of ultrafine-grained nickel, Mater. Sci. Eng. A 391 (2005) 377–389.
[17] M. Muzyk, Z. Pakiela, K.J. Kurzydlowski, Ab initio calculations of the generalized stacking fault energy in aluminium alloys, Scr. Mater. 64 (2011) 916–918.
[18] S. Qu, X.H. An, H.J. Yang, C.X. Huang, G. Yang, Q.S. Zang, Z.G. Wang, S.D. Wu, Z.F. Zhang, Microstructural evolution and mechanical properties of Cu-Al alloys subjected to equal channel angular pressing, Acta Mater. 57 (2009) 1586–1601.
[19] Y.H. Zhao, X.Z. Liao, Y.T. Zhu, Z. Horita, T.G. Langdon, Influence of stacking fault energy on nanostructure formation under high pressure torsion, Mater. Sci. Eng. A 410–411 (2005) 188–193.

[20] Y.B. Wang, Y.B. Wang, X.Z. Liao, Y.H. Zhao, E.J. Lavernia, S.P. Ringer, Z. Horita, T.G. Langdon, Y.T. Zhu, Stacking fault/twin boundary effect on grain refinement induced by high-pressure torsion in Cu-30wt% Zn, Mater. Sci. Eng. A 527 (2010) 4959–4966.
[21] S. Ni, Y.B. Wang, X.Z. Liao, H.Q. Li, R.B. Figueiredo, S.P. Ringer, T.G. Langdon, Y.T. Zhu, Effect of grain size on the competition between twinning and detwinning in nanocrystalline metals, Phys. Rev. B 84 (2011) 235401.
[22] J.Y. Zhang, G. Liu, R.H. Wang, J. Li, J. Sun, E. Ma, Double-inverse grain size dependence of deformation twinning in nanocrystalline Cu, Phys. Rev. B 81 (2010) 172104.
[23] Z.W. Wang, Y.B. Wang, X.Z. Liao, Y.H. Zhao, E.J. Lavernia, Y.T. Zhu, Z. Horita, T.G. Langdon, Influence of stacking fault energy on deformation mechanism and dislocation storage capacity in ultrafine-grained materials, Scr. Mater. 60 (2009) 52–55.
[24] Y. Zhang, N.R. Tao, K. Lu, Effect of stacking-fault energy, strain rate and temperature on microstructure and strength of nanostructured Cu-Al alloys subjected to plastic deformation, Acta Mater. 59 (2011) 6048–6058.
[25] C.B. Carter, I.L.F. Ray, On the stacking-fault energies of copper alloys, Philos. Mag. 35 (1977) 189–200.
[26] F.J. Humphreys, M.M. Hatherly, Recrystallization and Related Annealing Phenomena, Elsevier, Oxford, 2004.
[27] G.E. Dieter, Mechanical Metallurgy, McGraw-Hill, Boston, 1986.
[28] Y.S. Li, L.J. Dai, Y. Cao, Y.H. Zhao, Y.T. Zhu, Grain size effect on deformation twin thickness in ananocrystalline metal with low stacking-fault energy, J. Mater. Res. 194 (2019) 2398–2405.
[29] S. Mahajan, G.Y. Chin, Formation of deformation twins in fcc crystals, Acta Metall. 21 (1973) 1353–1363.
[30] J.J. Gilman, Mechanism of the Koehler dislocation multiplication process, Philos. Mag. 76 (1997) 329–336.
[31] M.A. Meyers, O. Vöhringer, V.A. Lubarad, The onset of twinning in metals: a constitutive description, Acta Mater. 49 (2001) 4025–4039.
[32] S. Mahajan, Critique of mechanisms of formation of deformation, annealing and growth twins: face-centered cubic metals and alloys, Scr. Mater. 68 (2013) 95–99.
[33] V. Yamakov, D. Wolf, S.R. Phillpot, A.K. Mukherjee, H. Gleiter, Deformation-mechanism map for nanocrystalline metals by molecular-dynamics simulation, Nat. Mater. 3 (2004) 43–47.
[34] F.A. Mohamed, Adislocation model for the minimum grain size obtainable by milling, Acta Mater. 51 (2003) 4107–4119.
[35] U.F. Kocks, H. Mecking, Physics and phenomenology of strain hardening: the FCC case, Prog. Mater. Sci. 48 (2003) 171–273.
[36] D. Hull, D.J. Bacon, Introduction to dislocation, University of Liverpool. University, Liverpool, 2011, pp. 99–102.
[37] X.Z. Gao, Y.P. Lu, J.Z. Liu, J. Wang, T.M. Wang, Y.H. Zhao, Extraordinary ductility and strain hardening of $Cr_{26}Mn_{20}Fe_{20}Co_{20}Ni_{14}$ TWIP high-entropy alloy by cooperative planar slipping and twinning, Materialia 8 (2019) 100485.
[38] X.H. An, S.D. Wu, Z.G. Wang, Z.F. Zhang, Significance of stacking fault energy in bulk nanostructured materials: insight from Cu and its binary alloys ad model systems, Prog. Mater. Sci. 48 (2019) 1–45.
[39] A. Mishra, B.K. Kad, F. Gregori, M.A. Meyers, Microstructural evolution in copper subjected to severe plastic deformation: experiments and analysis, Acta Mater. 55 (2007) 13–28.
[40] L.E. Murr, Interfacial Phenomena in Metals and Alloys, Addison-Wesley, New York, 1976.
[41] Y. Cao, Y.B. Wang, X.H. An, X.Z. Liao, M. Kawasaki, S.P. Ringer, T.G. Langdon, Y.T. Zhu, Grain boundary formation by remnant dislocations from the de-twinning of thin nano-twins, Scr. Mater. 100 (2015) 98–101.
[42] Y. Cao, Y.B. Wang, X.H. An, X.Z. Liao, M. Kawasaki, S.P. Ringer, T.G. Langdon, Y.T. Zhu, Concurrent microstructural evolution of ferrite and austenite in a duplex stainless steel processed by high-pressure torsion, Acta Mater. 63 (2014) 16–29.
[43] J.P. Hirth, J. Lothe, Theory of Dislocations, Krieger, Malabar, UK, 1992, pp. 131–137.
[44] A. Seeger, M. Hoffmann, A generalized method for estimating multiaxial elastic plastic notch stresses and strains, J. Eng. Mater. Technol. 107 (1985) 255–260.
[45] P. Zhang, S. Qu, M.X. Yang, G. Yang, S.D. Wu, S.X. Li, Z.F. Zhang, Varying tensile fracture mechanisms of Cu and Cu-Zn alloys with reduced grain size: from necking to shearing instability, Mater. Sci. Eng. A 594 (2014) 309–320.
[46] X.L. Ma, H. Zhou, J. Narayan, Y.T. Zhu, Stacking-fault energy effect on zero-strain deformation twinning in nanocrystalline Cu-Zn alloys, Scr. Mater. 109 (2015) 89–93.
[47] X.L. Wu, Y.T. Zhu, Inverse grain-size effect on twinning in nanocrystalline Ni, Phys. Rev. Lett. 101 (2008) 025503.
[48] S.S. Sohn, S. Hong, J. Lee, B.C. Suh, S.K. Kim, B.J. Lee, N.J. Kim, S. Lee, Effects of Mn and Al contents on cryogenic-temperature tensile and Charpy impact properties in four austenitic high-Mn steels, Acta Mater. 100 (2015) 39–52.
[49] S. Curtze, V.T. Kuokkala, Dependence of tensile deformation behavior of TWIP steels on stacking fault energy, temperature and strain rate, Acta Mater. 58 (2010) 5129–5141.
[50] M.W. Chen, E. Ma, K.J. Hemker, H.W. Sheng, Y.M. Wang, X.M. Cheng, Deformation twinning in nanocrystalline aluminum, Science 300 (2003) 1275–1277.
[51] X.Z. Liao, F. Zhou, E.J. Lavernia, S.G. Srinivasan, M.I. Baskes, D.W. He, Y.T. Zhu, Deformation mechanism in nanocrystalline Al: partial dislocation slip, Appl. Phys. Lett. 83 (2003) 632.
[52] H.W. Zhang, X. Huang, N. Hansen, Evolution of microstructural parameters and flow stresses toward limits in nickel deformed to ultra-high strains, Acta Mater. 56 (2008) 5451–5465.